Flight Simulation of a Swashplateless Helicopter using Rotor RPM Variation and Movable CG

Jayanth Krishnamurthi [*] **Anand Gandhi** [†]

Department of Mechanical, Aerospace, and Nuclear Engineering
Rensselaer Polytechnic Institute
Troy, NY 12180, USA

Abstract

This paper focuses on swashplateless primary control of a helicopter using rotor RPM variation in lieu of rotor collective pitch, and longitudinal and lateral cg motion in lieu of rotor cyclic pitch. Using a model of a swashplateless variant of the UH-60A Black Hawk helicopter, trim results over a range of airspeeds and flight simulation results for the aircraft as it transitions from hover to 70 knots cruise are presented. In the absence of rotor longitudinal cyclic pitch, the rotor tip path plane tilts further back (increasingly negative β_{1c}) with increasing cruise speed, while the aircraft assumes a heavy nose-down pitch attitude so the rotor can provide a propulsive thrust. Using the horizontal tail slew schedule of the baseline aircraft, a total forward cg travel of 2.48 ft, from the hover position, is required to operate at 120 knots. However, if the horizontal tail slew schedule is modified so that it introduces nose-down pitching moments on the aircraft at higher airspeeds, the required cg travel can be reduced to as little as 0.77 ft for operation from hover to 120 knots cruise. Flight simulation results were carried out in two steps – hover to 40 knots transition flight, and 40 knots to 70 knots cruise corresponding to low power cruise operation, each over a 60 sec interval. The flight simulation results showed that the inertial velocities of the aircraft are well regulated by the controller, and the steady-state values of the controls and rotor flapping at the end of each "maneuver" compare well with the calculated trim values at the speeds achieved.

1. INTRODUCTION

In recent years there has been much interest in alternate methods for helicopter primary control that do not rely on the use of the conventional main rotor swashplate mechanism. Although well established and reliable, the swashplate is heavy, complex, highly maintenance intensive, and a source of much aerodynamic drag in cruise and high-speed flight. A swashplateless primary control system can, in principle, reduce rotor hub complexity, aerodynamic drag and maintenance requirements tremendously. The earliest efforts by Straub and Charles in 1990[1], followed by those of Ormiston nearly a decade later[2], and more recent comprehensive studies by Shen and Chopra[3,4,5,6,7], and Falls, Datta and Chopra[8,9,10] all focused on the use of trailing-edge flaps (TEFs) on rotor blades for primary control, in lieu of the swashplate mechanism.

From all of the above studies a number of lessons were learned with regards to TEF enabled swashplateless primary control. First, the torsional frequency of the rotor has to be reduced, generally to 2/rev or lower, so that the aerodynamic pitching moments generated by the TEF can produce the required blade pitch variations. Second, pitch-indexing is necessary to limit the required TEF deflections to trim the aircraft. Third, the TEF chord and span dimensions and the deflection requirements are significantly greater than required for vibration and noise reduction, with the deflections required in high-speed and maneuvers typically exceeding that achievable with piezoelectric actuators (preferred for rotor applications). It was shown by Gandhi, Duling, and Straub[11] that the large TEFs, and the deflections required for primary control, result in a significant aerodynamic drag and power penalty. Based on a study conducted by Gandhi and Sekula[12] which demonstrated that cyclic pitch requirements in high-speed flight on a conventionally controlled rotor could

[*] Graduate Research Assistant
[†] Visiting Researcher, Shaker High School, Latham, NY
Presented at the 41st European Rotorcraft Forum, Munich, Germany, Sept. 1-4, 2015

be reduced through the use of a movable horizontal tail, Bluman and Gandhi[13] proceeded to show that a movable tail could limit TEF deflection requirements in a swashplateless configuration. Another approach, considered in the study by Sekula and Wilbur[14], was to use separate flaps on the blades for rotor collective and cyclic control.

An altogether different approach to swashplateless primary control, eschewing the use of on-blade TEFs, was presented by Gandhi, Yoshizaki, and Sekula[15]. In this study, the authors proposed using rotor RPM variation in lieu of collective pitch control and moving the aircraft center-of-gravity (CG) in lieu of cyclic pitch control. The CG could be moved, for example, by placing a fuel tank, batteries or payload on tracks and using actuators to move them in the fore-aft and lateral directions. Results, based on a swashplateless variant of a Robinson R22 type aircraft, showed that trim could be achieved at high speeds, and forward CG movement requirements could be reduced by introducing a forward tilt of the rotor shaft or setting the horizontal tail at a nose-up angle of attack relative to the aircraft waterline. Using a model of a swashplateless variant of the UH-60A Black Hawk helicopter, the current study represents a continuation of the effort reported in Ref. 15. However, in addition to trim results over a range of airspeeds achieved with RPM variation and CG movement, flight simulation results are presented for the aircraft as it transitions from hover to cruise, and comparisons with the baseline aircraft (with conventional controls) as well as detailed discussions and physical insights are provided.

2. SIMULATION MODEL

A simulation model for the UH-60A Black Hawk has been developed in-house, with components based on Sikorsky's GenHel model[16].The model is a non-linear, blade element representation of a single main rotor with articulated blades and table look-up for airfoil aerodynamic coefficients. The blades themselves are individually formulated as rigid bodies undergoing rotations about an offset flapping hinge. The lag degree of freedom is neglected. The 3-state Pitt-Peters dynamic inflow model[17] is used to represent the induced velocity distribution on the rotor disk. The tail rotor forces and torque are based on the closed-form Bailey rotor model[18]. The rigid fuselage and empennage (horizontal and vertical tail) forces and moments are implemented as look-up tables based on wind tunnel data from the GenHel model[16]. A simple 3-state generic turbine engine model given by Padfield[19] is used for the propulsion dynamics, with the governing time constants approximated based on the GenHel engine model[16].

The nonlinear dynamics for the baseline aircraft are written as

$$\dot{\vec{x}} = f(\vec{x}, \vec{u}_1) \tag{1}$$
$$\vec{y} = g(\vec{x}, \vec{u}_1)$$

where $\vec{y}$ is a generic output vector. The state vector, $\vec{x}$, is given by

$$\vec{x} = [u, v, w, p, q, r, \phi, \theta, \psi, X, Y, Z, \tag{2}$$
$$\beta_0, \beta_{1s}, \beta_{1c}, \beta_d, \dot{\beta}_0, \dot{\beta}_{1s}, \dot{\beta}_{1c}, \dot{\beta}_d, \lambda_0, \lambda_{1s}, \lambda_{1c},$$
$$\Omega, \chi_f, Q_e]^T$$

The state vector comprises of 12 fuselage states (3 body velocities (u, v, w), 3 rotational rates (p, q, r), 3 attitudes (ϕ, θ, ψ), and 3 inertial positions (X, Y, Z)), 11 rotor states (4 blade flapping states $(\beta_0, \beta_{1s}, \beta_{1c}, \beta_d)$ and their derivatives in multi-blade coordinates, and 3 rotor inflow states $(\lambda_0, \lambda_{1s}, \lambda_{1c})$) and 3 propulsion states (rotational speed (Ω), engine fuel flow (χ_f) and engine torque (Q_e)). The control input vector for the baseline aircraft is given by

$$\vec{u}_1 = [\delta_{lat}, \delta_{long}, \delta_{coll}, \delta_{ped}, \delta_{tht}]^T \tag{3}$$

and is comprised of lateral, longitudinal, and collective control inputs to the main rotor, pedal input to the tail rotor, and throttle input to the engine.

2.1. Baseline Model Validation

The baseline simulation model was validated against a trim sweep of flight test and GenHel data[20]. Figure 1 shows representative results and the baseline simulation model correlates well with both flight test and GenHel.

For the design of control laws, the nonlinear equations of motion were linearized using numerical perturbation at specific operating conditions. The linearized version of Equation 1 can be written as

$$\Delta\dot{\vec{x}} = A\Delta\vec{x} + B_1\Delta\vec{u}_1 \tag{4}$$
$$\Delta\vec{y} = C\Delta\vec{x} + D_1\Delta\vec{u}_1$$

The linearized model was subsequently validated against GenHel[20] and flight data[21] and Figure 2 shows representative results for hover and 80 knots forward flight. The model correlates fairly well in the frequency range of 0.4-10 rad/sec for both cases, as shown.

2.2. Primary Control through RPM Variation and CG Movement

On the baseline UH-60A, the control inputs δ_{lat}, δ_{long}, δ_{coll}, and δ_{ped} given in Equation 3 are passed through a mixing unit to determine the corresponding swashplate values (θ_{1c}, θ_{1s}, θ_0) and tail rotor pitch $\theta_{0_{TR}}$. The baseline UH-60A simulation model is now modified by removing the mixing unit and the swashplate inputs to the main rotor. The lateral and longitudinal control inputs are now directly mapped to lateral (Y_{CG}) and longitudinal (X_{CG}) CG movement.

The collective input is replaced by the throttle to regulate the rotor RPM. In the model given by Equation 1 and Equation 4, note that the rotor RPM is not a *direct* function of throttle input. Rather, the throttle input is mapped to the fuel flow state χ_f, where a change in this state induces a change in engine torque Q_e, which then induces a change in rotor RPM Ω.

The control input vector (and the associated mapping) is now given by

(5)
$$\vec{u}_2 = [\delta_{lat}, \delta_{long}, \delta_{tht}, \delta_{ped}]^T \Rightarrow [Y_{CG}, X_{CG}, \chi_f, \theta_{0_{TR}}]^T$$

With this new control input vector, the non-linear model given by Equation 1 and the linear model given by Equation 4 are now modified to

(6)
$$\begin{aligned} \dot{\vec{x}} &= f(\vec{x}, \vec{u}_2) \\ \vec{y} &= g(\vec{x}, \vec{u}_2) \end{aligned}$$

(7)
$$\begin{aligned} \Delta\dot{\vec{x}} &= A\Delta\vec{x} + B_2\Delta\vec{u}_2 \\ \Delta\vec{y} &= C\Delta\vec{x} + D_2\Delta\vec{u}_2 \end{aligned}$$

3. CONTROL SYSTEM DESIGN

The design of the control system is based on model following linear dynamic inversion (DI)[22]. Model following concepts are widely used in modern rotorcraft control systems for their ability to achieve task-tailored handling qualities via independently setting feed-forward and feedback characteristics[23]. In addition, the dynamic inversion controller does not require gain scheduling since it takes into account the nonlinearities and cross-couplings of the aircraft (i.e. a model of the aircraft is built into the controller). It is thus suitable for a wide range of flight conditions[22].

A schematic of the overall control system is shown in Figure 3. The control system is effectively split into inner and outer loop control laws (CLAWS). In designing the CLAWS, the full 26-state linear model given by Equation 7 was reduced to an 8-state quasi-steady model. Since the rotor dynamics are considerably faster than the fuselage dynamics, they can essentially be considered as quasi-steady states and folded into the fuselage dynamics[19], which reduces computational cost. The dynamic propulsion states are also folded into the fuselage dynamics to further reduce computational cost. The resulting system is an effective 8-state quasi-steady model whose state and control vectors are given by

(8)
$$\begin{aligned} \Delta\vec{x}_r &= [\Delta u, \Delta v, \Delta w, \Delta p\, \Delta q, \Delta r, \Delta\phi, \Delta\theta]^T \\ \Delta\vec{u}_2 &= [\Delta(\delta_{lat}), \Delta(\delta_{long}), \Delta(\delta_{tht}), \Delta(\delta_{ped})]^T \end{aligned}$$

In this reduced-order model, the output vector is set up such that it contains only the states themselves or contains quantities which are a function of only the states. Therefore, the matrix D_2 given in Equation 7 is eliminated from the model structure. In addition, while the controller uses a reduced-order linear model, its performance was ultimately tested with the full nonlinear model given by Equation 6.

3.1. Inner Loop CLAW

A diagram of the inner loop CLAW is shown in Figure 4. In the inner loop, the response type to pilot input is designed for Attitude Command Attitude Hold (ACAH) in the roll and pitch axis, where pilot input commands a change in roll and pitch attitudes ($\Delta\phi_{cmd}$ and $\Delta\theta_{cmd}$) and returns to the trim values when input is zero. The heave axis response type is designed for Vertical Speed Command Height Hold (VCHH), where pilot input commands a change in rate-of-climb and holds current height when the rate-of-climb is zero. The yaw axis response type is designed for Rate Command Heading Hold (RCHH), where pilot input commands a change in yaw rate and holds current heading when yaw rate is zero. These are based on ADS-33E specifications for hover and low-speed forward flight ($V \leq 45$ knots)[24].

The commanded values (shown in Figure 4) are given by

(9)
$$\Delta\vec{y}_{inner,cmd} = \begin{bmatrix} \Delta\phi_{cmd} \\ \Delta\theta_{cmd} \\ \Delta V_{Z_{cmd}} \\ \Delta r_{cmd} \end{bmatrix}$$

They are subsequently passed through command filters, which generate the reference trajectories ($\Delta\vec{y}_{ref}$) and their derivatives ($\Delta\dot{\vec{y}}_{ref}$) (see Figure 4). The parameters of the command filter were selected to meet Level 1 handling qualities specifications (bandwidth and phase delay) given by ADS-33E for small amplitude response in hover and low-speed forward flight[24]. Table 1

shows the parameters used in the command filters in the inner loop CLAW, where the roll and pitch axes use second-order filters and the heave and yaw axes use first-order filters.

Table 1: Inner Loop Command Filter Parameters

Command Filter	ω_n (rad/sec)	ζ	τ (sec)
Roll	2.5	0.8	-
Pitch	2.5	0.8	-
Heave	-	-	2
Yaw	-	-	0.4

In dynamic inversion, the technique of input-output feedback linearization is used, where the output equation ($\Delta\vec{y}_{inner}$ in Equation 10) is differentiated until the input appears explicitly in the derivative[22,25]. The inversion model implemented in the controller uses the 8-state vector given by Equation 8. Writing the reduced-order linear model in state space form, we have

$$\Delta\dot{\vec{x}}_r = A_r\Delta\vec{x}_r + B_r\Delta\vec{u}_2 \qquad \Delta\vec{y}_{inner} = C_r\Delta\vec{x}_r \tag{10}$$

where the A_r matrix is 8x8, B_r is 8x4, C_r matrix is 4x8, and the output vector $\Delta\vec{y}_{inner}$ is 4x1. The matrices A_r and B_r used in Equation 10 are scheduled with airspeed.

Applying dynamic inversion on Equation 10 results in the following control law

$$\Delta\vec{u}_2 = \left[C_r A_r^{k-1} B_r\right]^{-1}\left(\nu - \left[C_r A_r^{k}\right]\Delta\vec{x}_r\right) \tag{11}$$

where k = 2 for the roll and pitch axes, and k = 1 for the heave and yaw axes. The term ν is known as the "pseudo-command" vector or an auxiliary input vector, shown in Figure 4. The psuedo-command vector is a sum of feedforward and feedback components. It is defined as

$$\nu = \begin{bmatrix}\nu_\phi \\ \nu_\theta \\ \nu_{V_Z} \\ \nu_r\end{bmatrix} = \Delta\dot{\vec{y}}_{ref} + [K_P\ K_D\ K_I]\begin{bmatrix} e \\ \dot{e} \\ \int e\,dt\end{bmatrix} \tag{12}$$

where the error vector, denoted as e (see Figure 4) is given by

$$e = \Delta\vec{y}_{ref} - \Delta\vec{y}_{inner} \tag{13}$$

The variables K_P,K_D, and K_I indicate the proportional, derivative, and integral gains in a PID compensator.

Note that the application of dynamic inversion in Equation 10 is carried out in the body reference frame. In Equation 12, the pseudo-commands ν_ϕ, ν_θ, and ν_r are prescribed in the body frame, while ν_{V_Z} is in the inertial frame. Therefore, a transformation was introduced to change the heave axis pseudo-command to the body frame[26] prior to inversion, and is given by

$$\nu_w = \frac{\nu_{V_Z} + u\dot{\theta}\cos\theta}{\cos\theta\cos\phi} \tag{14}$$

If the reduced-order model given by Equation 10 were a perfect representation of the flight dynamics, the resulting system after inversion would behave like a set of integrators and the pseudo-command vector would not require any feedback compensation. In practice, however, errors between reference and measured values arise due to higher-order vehicle dynamics and/or external disturbances and therefore require feedback to ensure stability.

The PID compensator gains are selected to ensure that the tracking error dynamics due to disturbances or modeling error are well regulated. A typical choice for the gains is that the error dynamics be on the same order as that of the command filter model for each axis. Table 2 shows the compensator gain values used in each axis.

Table 2: Inner Loop Error Compensator Gains

	K_P	K_D	K_I
Roll	10 (1/sec^2)	5.75 (1/sec)	4.6875 (1/sec^2)
Pitch	10 (1/sec^2)	5.75 (1/sec)	4.6875 (1/sec^2)
Heave	1 (1/sec)	0	0.25 (1/sec^2)
Yaw	1 (1/sec)	0	6.25 (1/sec^2)

Finally, the vector $\Delta\vec{u}_2$ from Equation 11 is added to the trim values of $\vec{u}_2$, which are scheduled with airspeed, before being passed into the aircraft.

3.2. Outer Loop CLAW

In order to maintain trimmed forward flight, an outer loop is designed to regulate lateral (V_Y) and longitudinal (V_X) ground speed. A schematic of the outer loop CLAW is shown in Figure 5. Note that the overall structure is similar to the inner loop. The response type for the outer loop is translational rate command, position hold (TRC/PH), where pilot input commands a change in ground speed and holds current inertial position when ground speeds are zero. With the implementation of the outer loop, the pilot input does not directly command $\Delta\phi_{cmd}$ and $\Delta\theta_{cmd}$ as in the inner loop CLAW.

Rather, they are indirectly commanded through the desired ground speeds (see Figure 3).

The commanded values in the outer loop (shown in Figure 5) are given by

$$\Delta\vec{y}_{outer,cmd} = \begin{bmatrix} \Delta V_{X_{cmd}} \\ \Delta V_{Y_{cmd}} \end{bmatrix} \tag{15}$$

and passed through first-order command filters. Similar to the inner loop, the parameters of the command filter are selected based on ADS-33E specifications in hover and low-speed forward flight[24].

Table 3: Outer Loop Command Filter Parameters

Command Filter	τ (sec)
Lateral (V_Y)	2.5
Longitudinal (V_X)	2.5

In the outer loop, to achieve the desired ground speeds, the required pitch and roll attitude command input to the inner loop (Equation 9) is determined through model inversion[22,27]. A simplified linear model of the lateral and longitudinal dynamics is extracted from Equation 10 and is given by

$$\begin{aligned} \Delta\dot{\vec{x}}_{r,outer} &= A_{TRC}\Delta\vec{x}_{r,outer} + B_{TRC}\begin{bmatrix} \Delta\phi_{cmd} \\ \Delta\theta_{cmd} \end{bmatrix} \\ \Delta\vec{y}_{outer} &= \begin{bmatrix} \Delta V_X \\ \Delta V_Y \end{bmatrix} = C_{TRC}\Delta\vec{x}_{r,outer} \end{aligned} \tag{16}$$

with A_{TRC}, B_{TRC}, and $\Delta\vec{x}_{r,outer}$ defined as

$$\begin{aligned} A_{TRC} &= \begin{bmatrix} X_u & X_v \\ Y_u & Y_v \end{bmatrix} \\ B_{TRC} &= \begin{bmatrix} 0 & -g \\ g & 0 \end{bmatrix} \\ \Delta\vec{x}_{r,outer} &= \begin{bmatrix} \Delta u \\ \Delta v \end{bmatrix} \end{aligned} \tag{17}$$

where u and v are body-axis velocities, X_u, X_v, Y_u, and Y_v are stability derivatives and g is the gravitational acceleration. Applying dynamic inversion on this model results in the following control law

$$\begin{bmatrix} \Delta\phi_{cmd} \\ \Delta\theta_{cmd} \end{bmatrix} = (C_{TRC}B_{TRC})^{-1}\left(\nu - C_{TRC}A_{TRC}\Delta\vec{x}_{r,outer}\right) \tag{18}$$

The pseudo-command vector, $\nu = \begin{bmatrix} \nu_{V_X} \\ \nu_{V_Y} \end{bmatrix}$, is defined similarly to Equation 12, with the error dynamics also defined in a manner similar to that of the inner loop. The PID compensator gains for the outer loop are given in Table 4.

Table 4: Outer Loop Error Compensator Gains

	K_P (1/sec)	K_D	K_I (1/sec^2)
Lateral (V_Y)	0.8	0	0.16
Longitudinal (V_X)	0.8	0	0.16

4. RESULTS & DISCUSSION

The results in this study are based on a model developed to represent a swashplateless variant of the UH-60A Black Hawk helicopter. The swashplateless helicopter is identical to the baseline UH-60A helicopter (key properties provided in Table 5) with the following exceptions. The main rotor collective and cyclic pitch control is eliminated, but the root collective pitch is set at a fixed (index) value of $18.56°$, corresponding to the value in hover for the reference aircraft operating at a rotor speed of 258 RPM. The swashplateless variant has provisions for rotor RPM variation and cg movement in the longitudinal and lateral directions.

In Figure 6, the longitudinal cg position for the baseline aircraft is shown at 30 ft from the reference point, placing the cg 1.57 ft aft of the rotor hub. To trim the aircraft in hover without main rotor cyclic pitch, the longitudinal position of the cg is required to be at 29.44 ft from the rotor tip, as shown in Figure 6. This places the cg 1.01 ft aft of the rotor hub, or 0.56 ft forward of the cg for the baseline aircraft. For operational purposes, the longitudinal cg travel required from this position is of significance. Figure 7 shows the lateral cg position for the baseline aircraft and the swashplateless variant. For the baseline aircraft, the lateral cg offset relative to the rotor hub is zero. Trimming the swashplateless variant in hover without the use of main rotor cyclic pitch requires a 0.25 ft cg offset toward the port side, as shown in Figure 7. As the aircraft operational conditions change, the lateral cg travel required from this position is of important consideration.

The presentation and discussion of the results in is organized in four sub-sections. Section 4.1 covers trim conditions with airspeed variation for the swashplateless aircraft, and provides a comparison with the baseline aircraft. Section 4.2 provides flight simulation results for transition from hover to a forward flight speed of 40 knots. In Section 4.3, the effect of modifying the slew schedule of the horizontal tail on the aircraft trim are considered, and finally Section 4.4 covers flight simulation for the aircraft going from 40 knots to 70 knots

(minimum power cruise speed).

4.1. Swashplateless Aircraft Trim

Figures 8(a) and 8(b) show the variation of the longitudinal and lateral cg positions, respectively, to trim the aircraft over a 0-120 knots airspeed range. In Figure 8(a), the required longitudinal cg position moves forward by 2.44 ft, from 29.44 ft position for hover (see Figure 6), to the 27 ft position at 120 knots. In Figure 8(b), the lateral cg travel is seen to be relatively small (moving between 0.1-0.42 ft, port of the rotor hub). Figure 9 shows the required RPM variation, versus airspeed, to trim the aircraft. The RPM reduction as the aircraft transitions from hover to forward flight is consistent with the known reduction in a helicopter's induced power requirement, and drops down to a value of 211 RPM at a speed of around 70 knots (down from the 258 RPM requirement at hover). Also indicated on Figures 8(a) and 8(b) are the cg position, and on Figure 9 the rotor RPM, for the reference aircraft (with conventional controls).

Figures 10(a) and 10(b) show the pitch and roll attitudes, respectively, of the aircraft over the 0-120 knots airspeed range. The baseline aircraft hovers with a nose-up pitch attitude and flies nose-level at 120 knots. In comparison, the nose-up attitude in hover is smaller for the swashplateless variant, going to nose-level at 40 knots, and up to nearly 6 deg nose-down at 120 knots. In Figure 10(b) the roll-left attitude of the swashplateless aircraft in hover is seen to be greater than the baseline aircraft, and that trend persists to moderate speeds, before reversing.

The aircraft rpm, pitch and roll attitude are related to the rotor flapping response shown in Figure 11. The rotor coning (Figure 11(a)), seen to be substantially higher for the swashplateless configuration, is consistent with the lower rotor RPM in Figure 9, resulting in a reduced centrifugal force. The longitudinal cyclic flapping (Figure 11(b)) shows the rotor tip-path-plane tilting forward for the baseline aircraft (positive β_{1c}) but blowing back for the swashplateless configuration (negative β_{1c}). The blow-back phenomenon is a characteristic of any rotor in forward flight condition in the absence of longitudinal cyclic pitch to overcome it and force the tip-path plane to tilt forward. The increasing blow-back of the tip-path plane with increasing forward speed for the swashplateless configuration, in fact, necessitates the large nose-down pitch attitude of the aircraft (seen in Figure 10(a)) so that the rotor thrust vector has a net forward tilt to provide the required propulsive force. In Figure 11(c), the baseline aircraft has the rotor flapping downward to the left in hover (positive β_{1s}) to counteract the tail rotor thrust. This is achieved through the introduction of lateral cyclic pitch. With the inability to introduce lateral cyclic pitch, there is no lateral cyclic flapping in hover for swashplateless configuration. Instead, a leftward roll attitude of the aircraft (Figure 10(b)) in hover allows a component of the main rotor thrust to counteract the tail rotor thrust. With increasing forward speed, the coning of the rotor results in higher lift at the front of the disk and vice-versa, leading to the tendency of the rotor flapping downward to the right (negative β_{1s}). In the absence of any lateral cyclic pitch to compensate for this effect, and due to the larger coning it experiences (especially at moderate speeds, see Figure 11(a)), this phenomenon features prominently for the swashplateless configuration (see the larger negative β_{1s} values in Figure 11(c)).

4.2. Flight Simulation, Hover to 40 knots

This section provides flight simulation results for the aircraft as it transitions out of hover, to 40 knots. Although the baseline UH-60A Black Hawk helicopter with conventional swashplate control can accomplish this transition in just a few seconds, it is recognized that cg movement would require a larger time window with the details depending on the actuation system used. With the mechanism for cg movement unspecified in this study, it is very conservatively estimated that the required cg motion could be realized in 1 minute.

Figure 12 shows time histories of the aircraft velocities over the duration of the transition from hover to 40 knots. Note that the lateral and longitudinal ground speeds are controlled by the outer loop CLAW (section 3.2) while the vertical speed is controlled by the inner loop CLAW (section 3.1). As seen in the figure, they are well regulated by the controller. Figures 13(a) and 13(b) show time histories of the aircraft pitch and roll attitude, respectively, for both the baseline and the swashplateless configurations. As with the vertical speed, recall that the pitch and roll attitude are commanded by the inner loop CLAW. The actual attitude of the aircraft tracks well with that commanded by the inner loop CLAW. The differences between the baseline and swashplateless configurations were discussed in section 4.1. In Figure 13(a), the variation in aircraft pitch attitude during the transition from hover to 40 knots is heavily influenced by the interaction between the rotor wake and the horizontal tail. These interactions, predictably, have a smaller influence on the roll attitude of the aircraft (Figure 13(b)).

Time histories of the longitudinal and lateral cg positions for the aircraft to transition from hover to 40 knots over the 1 minute duration are shown in Figures 14(a) and 14(b), respectively. In Figure 14(a), the longitudinal cg is required to move forward from its hover position and then pull back partially. The steady-state value of

longitudinal cg position at 40 knots from the flight simulation in Figure 14(a) correlates well with the trim value at 40 knots from Figure 10(a). In Figure 14(b), the lateral cg position is seen to move further leftward from its hover position before pulling back partially. As with the longitudinal cg position, the steady-state value of lateral cg position at 40 knots from the flight simulation in Figure 14(b) correlates well with the trim value at 40 knots from Figure 10(b). Figure 15 shows the time history of the rotor speed as the aircraft transitions from hover to 40 knots. As with the lateral and longitudinal cg positions, the steady state value of rotor RPM at 40 knots compares well with the trim predictions from Figure 9.

Time histories of rotor blade coning, longitudinal flapping and lateral flapping are shown in Figures 16(a), 16(b) and 16(c), respectively. The coning increase in Figure 16(a) for the swashplateless configuration is attributed to the rotor RPM reduction (Figure 15). Without any rotor longitudinal cyclic pitch control, Figure 16(b) shows a smoothly increasing tip-path-plane blowback with time as the flight speed is increases for the swashplateless configuration. Similarly, Figure 16(c) shows a smoothly increasing lateral flapping (downward to the right), associated with increasing coning and increasing forward speed. The steady state values of rotor flapping response from the flight simulations in Figure 16 compare well with the trim prediction at 40 knots (Figure 11).

4.3. Horizontal Tail Slew Schedule Modification

In Figure 8(a), the required longitudinal cg position moves forward by 2.48 ft, going from hover to 120 knots. As an example, if the movable mass was 25% of the total mass of the aircraft, this would require 9.92 ft of forward motion. If the movable mass was reduced to 15%, the required forward motion would be a practically infeasible 16.53 ft. For cg variation to be a viable alternative to rotor cyclic pitch control, it is perhaps imperative to reduce the motion requirements. With this goal in mind, it is perhaps worth re-emphasizing that the purpose of the forward motion of the cg is to introduce a nose-down pitching moment on the aircraft and put it in a nose-down pitch attitude to provide the required propulsive thrust. The propulsive thrust requirement, and hence the forward cg movement, both increase with forward speed. This raises the point that the horizontal tail could be used at moderate to high-speeds, and its incidence adjusted to produce the required nose-down pitching moment on the aircraft. This could, in turn, relieve the forward cg movement requirement with increasing speed.

Figure 17(a) shows the longitudinal cg position required as a function of the horizontal tail incidence angle and the flight speed. The baseline slew schedule is indicated on the figure with the dashed line. Up to an airspeed close to 40 knots, the horizontal tail was set at high nose-up attitude to compensate for the impingement of the main rotor wake. Thereafter the horizontal tail incidence was steadily reduced, ending up at about 3 deg at 120 knots. The color contours show that using the baseline horizontal tail slew schedule, the cg is required to steadily move forward with increasing flight speed. If a different slew schedule was used, however, the cg movement requirements with forward speed could be significantly reduced. For example, the modified slew schedule indicated on Figure 17(a), which uses higher horizontal tail incidence angles at moderate to high-speeds, limits the cg motion requirement considerably. The longitudinal cg motion requirement versus airspeed for the baseline and modified slew schedule are more clearly seen on Figure 17(b). Beyond 40 knots, the baseline slew schedule requires the cg to steadily move forward. The modified slew schedule, on the other hand completely eliminates this requirement.

Trim results versus airspeed showed that using the modified slew schedule instead of the baseline slew schedule had no effect other than reducing the forward cg motion requirement (shown in Figure 17(b)). It was verified that the lateral CG motion, rotor RPM, aircraft pitch and roll attitude, rotor coning and longitudinal and lateral cyclic flapping, versus airspeed, were all virtually unchanged (results not included in the paper).

4.4. Flight Simulation, 40 to 70 knots

Previously, section 4.2 provided flight simulation results as the aircraft transitioned from hover to 40 knots over a 1 minute time duration. With minimum power (maximum endurance) at around 70 knots (Figure 1d), this section provides flight simulation results for the aircraft going from 40 to 70 knots, once again over a 60 second interval. For the results in this section, the error compensator gains used in heave axis for the inner loop (section 3.1) and the ground speeds in the outer loop (section 3.2) were modified to minimize transients observed at 70 knots. Table 6 shows the gains used.

Figure 18 shows time histories of the aircraft inertial velocities for the 60 second duration it transitions from 40 to 70 knots. While the longitudinal ground speed (Figure 18(a)) is very well regulated by the controller, both the lateral velocity (Figure 18(b)) and the vertical velocity (Figure 18(c)) show some transients in the time history. However, the transients are small, and are observed to settle quickly.

Figures 19(a) and 19(b), respectively, show time his-

tories of the longitudinal and lateral cg positions for the aircraft as it transition from 40 to 70 knots over a 1 min duration. In Figure 19(a), the cg is seen to move further forward corresponding to the baseline horizontal tail slew schedule, but retains its position when the modified slew schedule is used. The variation in the lateral cg position (Figure 19(b)) for both slew schedules is virtually the same. Figure 20 shows the time history of the rotor speed as the aircraft transitions from 40 to 70 knots. The steady state value of rotor RPM at 70 knots compares well with the trim predictions from Figure 9, and is virtually the same for both slew schedules considered.

Time histories of rotor blade longitudinal flapping are shown in Figure 21. The increasing blowback of the tip-path-plane over the 60 sec duration over which the aircraft speed is increasing from 40 to 70 knots is virtually identical, regardless of the horizontal tail slew schedule, and the longitudinal cyclic flapping at 70 knots correlates well with the trim results presented in Figure 11(b). This is not surprising when considering the fact that the horizontal tail and the aircraft cg, work in combination to get the aircraft into the same nose-down pitch attitude required to generate the propulsive thrust, and in the absence of any cyclic pitch control, the blowback will depend on aircraft pitch attitude and forward speed.

5. CONCLUSIONS

The current study examined swashplateless primary control of a helicopter using rotor RPM variation in lieu of rotor collective pitch, and longitudinal and lateral cg motion in lieu of rotor cyclic pitch. Results were presented for a swashplateless variant of the UH-60A Black Hawk helicopter, including trim results over a range of airspeeds and flight simulation results for the aircraft as it transitions from hover to 70 knots cruise. The flight simulations were carried out in two steps, from hover to 40 knots transition speed over a 60 sec duration, and 40 knots to 70 knots (minimum power speed) also over a 60 sec duration. From the results presented in the paper the following observations could be made:

1. For the baseline helicopter (with swashplate control) longitudinal cyclic pitch allows the rotor tip-path-plane to tilt forward even at moderate- to high-speed. For the swashplateless configuration, trim results show the rotor tip-path-plane blowing back as flight speed increases, requiring an increasing nose down pitch attitude of the aircraft (approaching 6 deg nose-down at 120 knots) so the rotor thrust can provide the required propulsive force.

2. With the fixed rotor collective pitch and rotor RPM for the swashplateless configuration matching the baseline aircraft values in hover, the rotor speed reduces to around 211 RPM as the speed increases to 70 knots, and increases slightly thereafter.

3. The lower rotor RPM requirement for the swashplateless configuration results in a higher blade coning, relative to the baseline aircraft. The higher coning, coupled with the lack of lateral cyclic pitch control, results in a right-downward tilt of the tip-path-plane.

4. For the swashplateless configuration, a total forward cg travel of 2.48 ft was required to trim the aircraft with increasing speed up to 120 knots. The lateral cg travel required was only 0.32 ft. By changing the horizontal tail slew schedule so it provided larger nose-down moments on the aircraft at moderate- to high-speed, the longitudinal cg travel requirements could be reduced to 0.77 ft.

5. Flight simulation results showed that the inertial velocities of the aircraft are well regulated by the controller.

6. Flight simulation results also showed that the steady-state values of the controls and rotor flapping at the end of each “maneuver” compared well with the calculated trim values at the speeds achieved.

References

[1] Straub, F., and Charles, B., ``Preliminary Assessment of Advanced Rotor/Control System Concepts (ARCS),'' Technical Report 90-D03, USA AVSCOM, 1990.

[2] Ormiston, R., ``Aeroelastic Considerations for Rotorcraft Primary Control with On-Blade Elevons,'' American Helicopter Society 57^{th} Annual Forum Proceedings, Washington, D.C., May 2001.

[3] Shen, J. and Chopra, I., ``Aeroelastic Stability of Trailing-Edge Flap Helicopter Rotors,'' *Journal of the American Helicopter Society*, vol. 48, pp. 236--243, October 2003. doi: 10.4050/JAHS.48.236.

[4] Shen, J. and Chopra, I., ``A Parametric Design Study for a Swashplateless Helicopter Rotor with Trailing-Edge Flaps,'' *Journal of the American Helicopter Society*, vol. 49, pp. 43--53, January 2004. doi:10.4050/JAHS.49.43.

[5] Shen, J. and Chopra, I., ``Aeroelastic Modeling of Trailing-Edge-Flap Helicopter Rotors Including Actuator Dynamics,'' *Journal of Aircraft*, vol. 41, pp. 1465--1472, November-December 2004. doi:10.2514/1.14431.

[6] Shen, J. and Chopra, I., ``Swashplateless Helicopter Rotor with Trailing-Edge Flaps,'' *Journal of Aircraft*, vol. 41, pp. 208--214, March-April 2004. doi: 10.2514/1.9279.

[7] Shen, J., Yang, M., and Chopra, I., ``Swashplateless Helicopter Rotor System with Trailing-Edge Flaps for Flight and Vibration Controls,'' *Journal of Aircraft*, vol. 43, pp. 346--352, April-May 2006. doi: 10.2514/1.14634.

[8] Falls, J., Datta, A., and Chopra, I., ``Integrated Trailing-Edge Flaps and Servotabs for Helicopter Primary Control,'' American Helicopter Society 62^{nd} Annual Forum Proceedings, Phoenix, AZ, May 2006 2006.

[9] Falls, J., Datta, A., and Chopra, I., ``Design and Analysis of Trailing Edge Flaps and Servotabs for Primary Control,'' American Helicopter Society 63^{rd} Annual Forum Proceedings, Virginia Beach, VA, May 1-3, 2007 2007.

[10] Falls, J., Datta, A., and Chopra, I., ``Performance Analysis of Trailing Edge Flaps in Helicopter Primary Control,'' Proceedings of the AHS Specialist's Conference on Aeromechanics, San Francisco, CA, January 2008 2008.

[11] Gandhi, F., Duling, C., and Straub, F., ``On Power and Actuation Requirement in Swashplateless Primary Control using Trailing Edge Flaps,'' *The Aeronautical Journal*, vol. 118, pp. 503--521, May 2014.

[12] Gandhi, F., and Sekula, M., ``Helicopter Horizontal Tail Incidence Control to Reduce Rotor Cyclic Pitch and Blade FlapFlap,'' Proceedings of the 60^{th} Annual Forum of the American Helicopter Society, Baltimore, MD, June.

[13] Bluman, J., and Gandhi, F., ``Reducing Trailing Edge Flap Deflection Requirements in Primary Control with a Moveable Horizontal Tail,'' *Journal of the American Helicopter Society*, vol. 56, no. 032005, 2011. doi:10.4050/JAHS.56.032005.

[14] Sekula, M.K., and Wilbur, M.L., ``Analysis of a Multi-Flap Control System for a Swashplateless Rotor,'' 2011.

[15] Gandhi, F., Yoshizaki, Y., and Sekula, M., ``Swashplateless Control of a Rotary-Wing UAV using Variable RPM and a Movable CG,'' Proceedings of the American Helicopter Society 62^{nd} Annual Forum, Phoenix, AZ, May 9-11 2006.

[16] Howlett, J.J., ``UH-60A Black Hawk Engineering Simulation Program: Volume I - Mathematical Model,'' NASA CR-166309, 1981.

[17] Peters, D.A., and HaQuang, N., ``Dynamic Inflow for Practical Applications,'' *Journal of the American Helicopter Society*, vol. 33, pp. 64--66, October 1988.

[18] Bailey, F.J., ``A Simplified Theoretical Method of Determining the Characteristics of a Lifting Rotor in Forward Flight,'' NACA Report 716, 1941.

[19] Padfield, G.D., *Helicopter Flight Dynamics: The Theory and Application of Flying Qualities and Simulation Modeling*. Blackwell Publishing, 2^{nd} ed., 2007.

[20] Ballin, M.G., ``Validation of a Real-Time Engineering Simulation of the UH-60A Helicopter,'' NASA TM-88360, 1987.

[21] Fletcher J.W., ``A Model Structure for Identification of Linear Models of the UH-60 Helicopter in Hover and Forward Flight,'' NASA TM-110362, NASA, 1995.

[22] Stevens, B.L. and Lewis, F.L., *Aircraft Control and Simulation*. John Wiley & Sons, 2^{nd} ed., 2003.

[23] Tischler, M.B. and Remple, R.K., *Aircraft and Rotorcraft System Identification: Engineering Methods with Flight Test Examples*. AIAA, 2^{nd} ed., 2012.

[24] Anonymous, ``Aeronautical Design Standard Performance Specification, Handling Qualities Requirements for Military Rotorcraft,'' ADS-33E-PRF, USAAMCOM, 2000.

[25] Slotine, J.E. and Li, W., *Applied Nonlinear Control*. Prentice-Hall Inc., 1991.

[26] Horn, J.F., and Guo, W., ``Flight Control Design for Rotorcraft with Variable Rotor Speed,'' Proceedings of the American Helicopter Society, 64^{th} Annual Forum, Montreal, Canada, April 29-May 1, 2008.

[27] Ozdemir, G.T., *In-Flight Performance Optimization for Rotorcraft with Redundant Controls*. PhD Thesis, The Pennsylvania State University, December 2013.

Table 5: UH-60 Helicopter Properties

Weight	W	18,300 lbs
Rotor Radius	R	26.8 ft
Blade Chord	c_b	1.73 ft
Angular Velocity	Ω	258 RPM
Shaft Tilt	α_s	3°
Solidity	σ	0.0822
Hinge Offset	e	1.25 ft
Blade Airfoil	-	SC1095/SC1094-R8 (varies spanwise)

Table 6: Error Compensator Gains, 40 to 70 knots

Compensator	Gains	Standard Slew Schedule	Modified Slew Schedule
V_Z	K_P	0.5	0.5
	K_I	0.05	0.05
V_X	K_P	0.8	0.4
	K_I	0.16	0.08
V_Y	K_P	0.4	0.08
	K_I	0.08	0.016

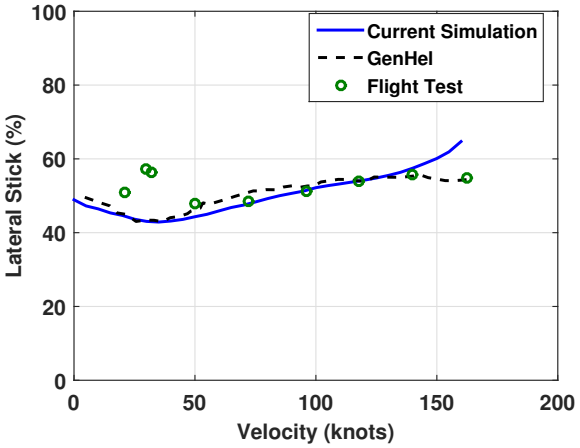

(a) Lateral Stick

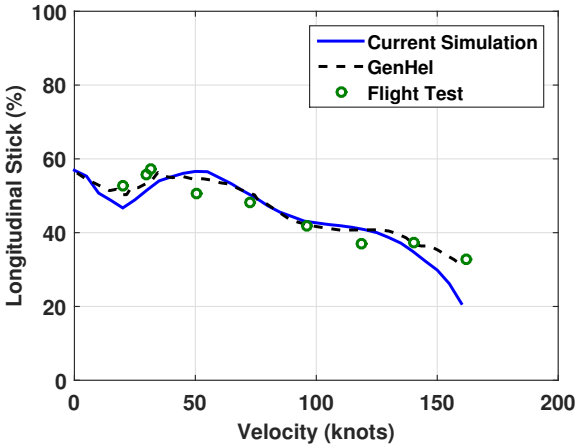

(b) Longitudinal Stick

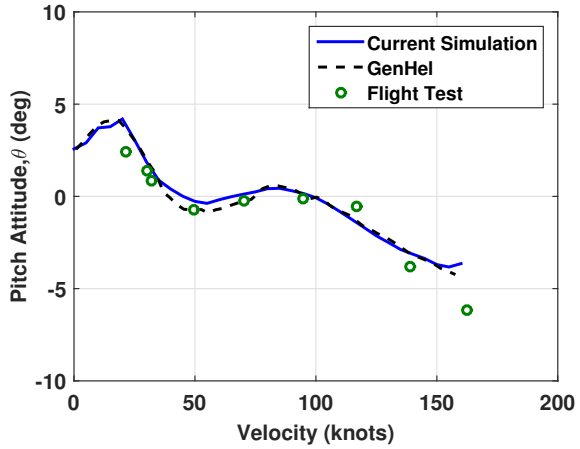

(c) Pitch Attitude

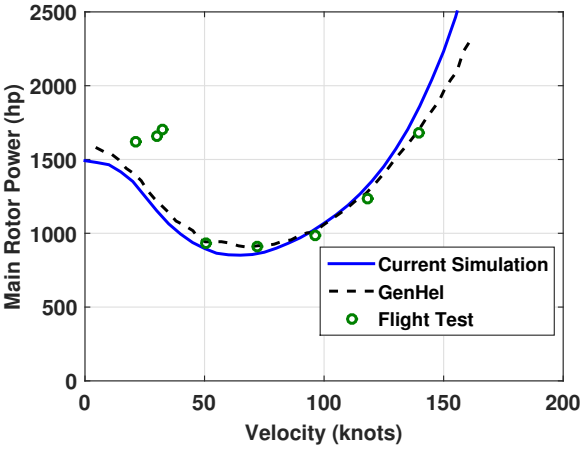

(d) Main Rotor Power

Fig. 1: Baseline UH-60A Trim Sweep Validation

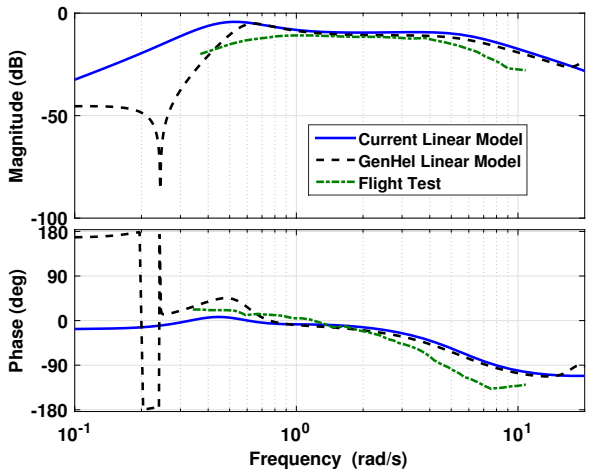

(a) Hover - p/δ_{lat}

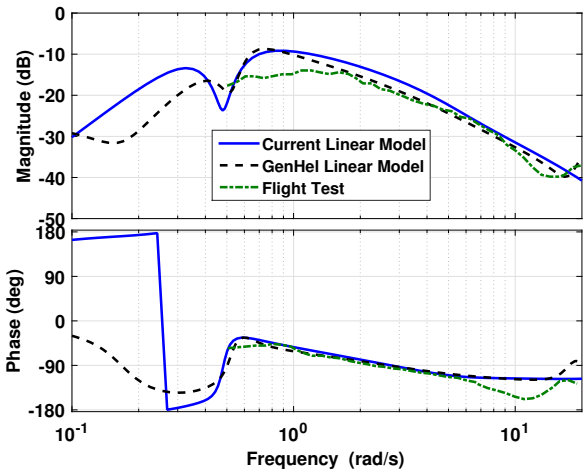

(b) Hover - q/δ_{long}

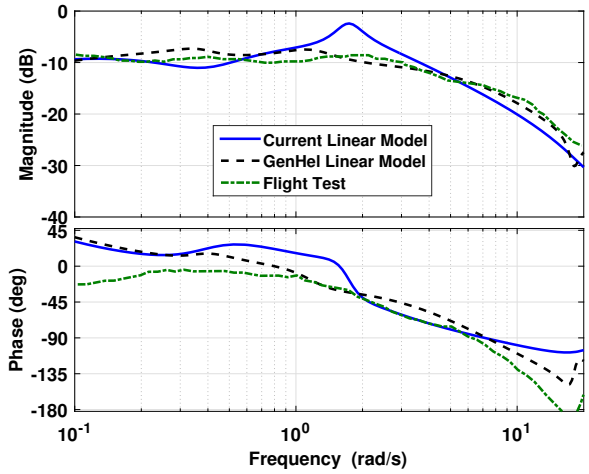

(c) 80 knots - p/δ_{lat}

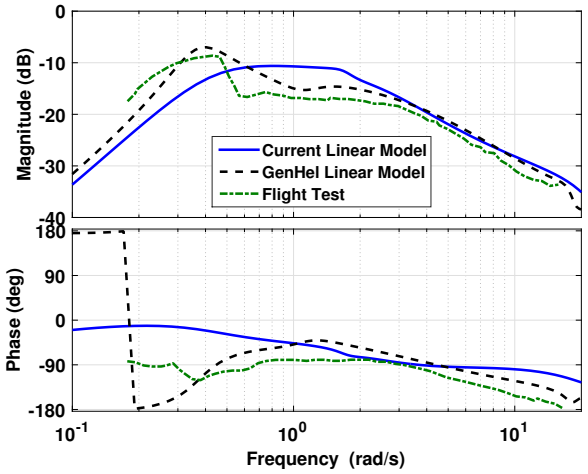

(d) 80 knots - q/δ_{long}

Fig. 2: Baseline UH-60A Frequency Response Validation

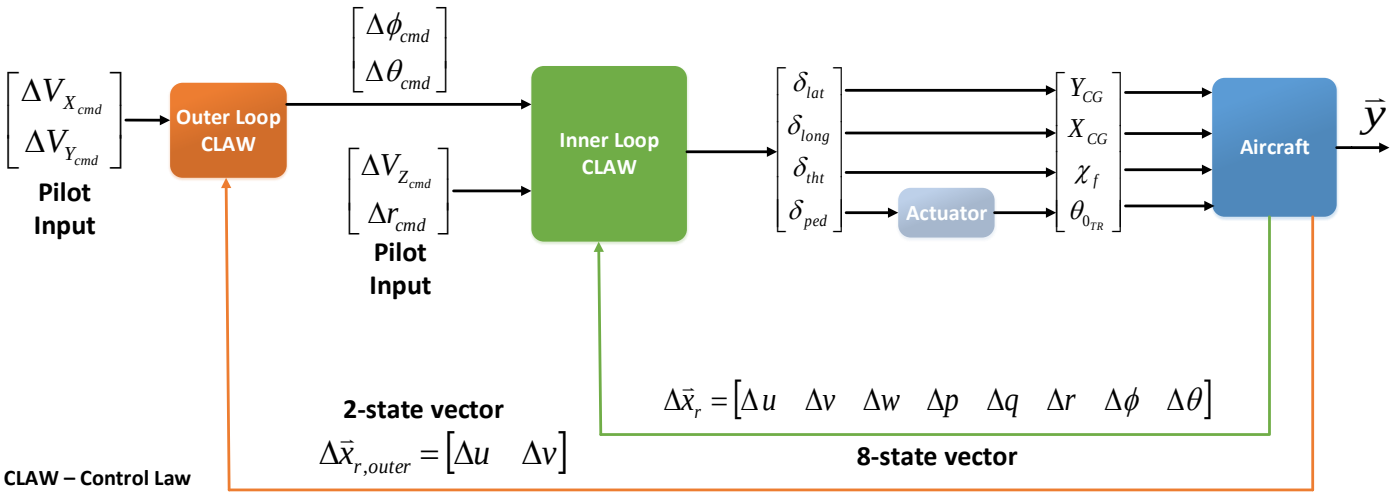

Fig. 3: Overview of the Control System

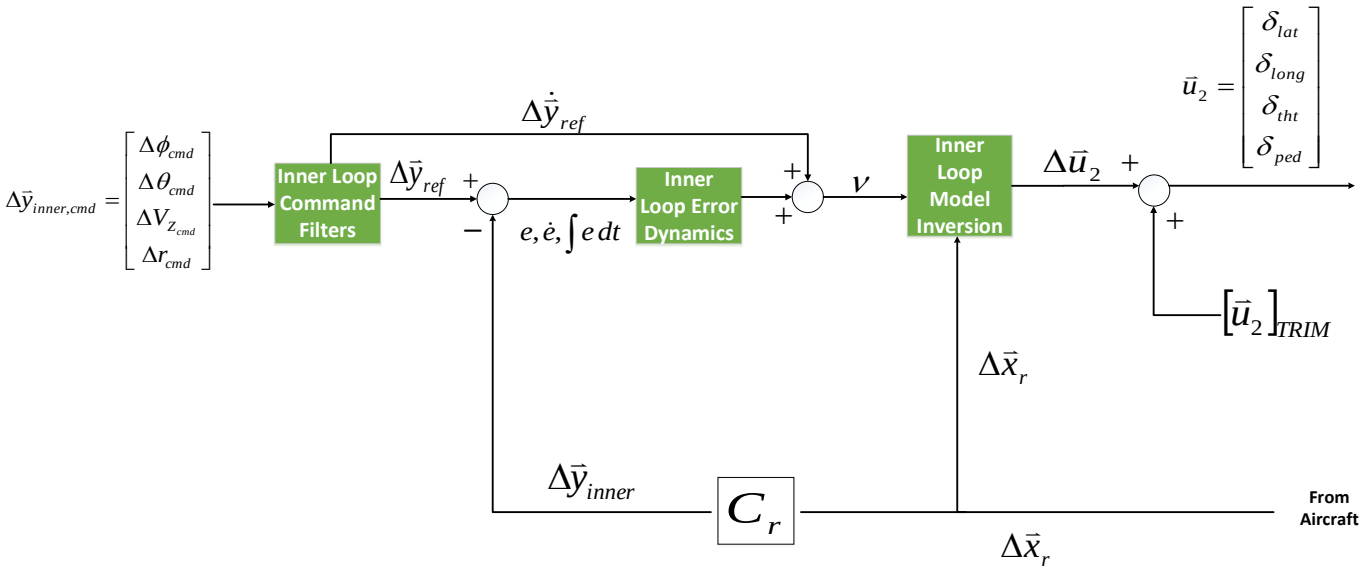

Fig. 4: Inner Loop CLAW

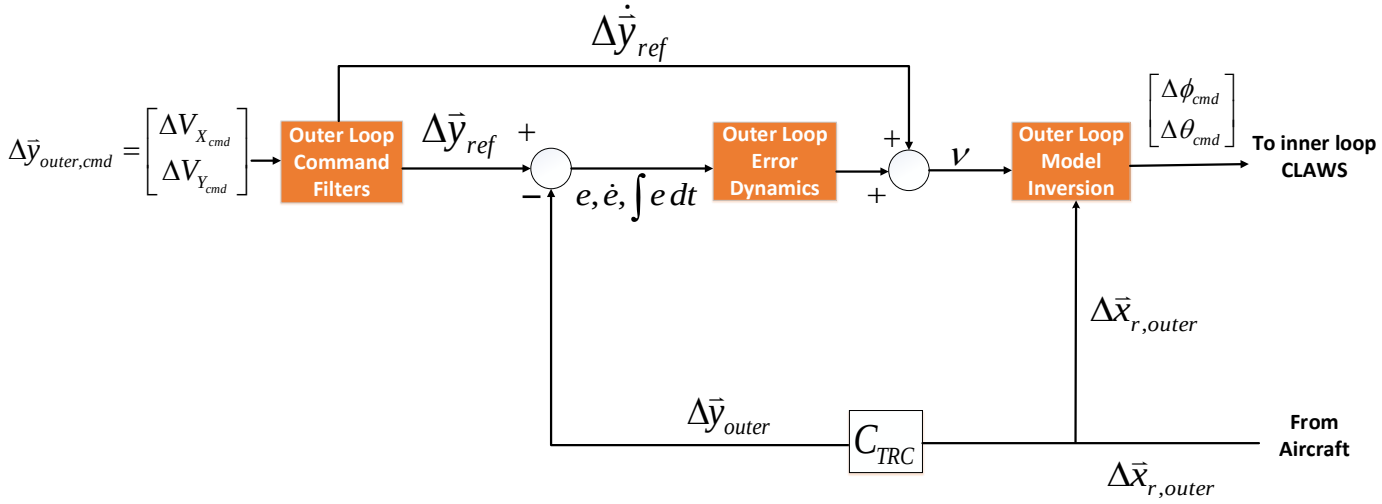

Fig. 5: Outer Loop CLAW

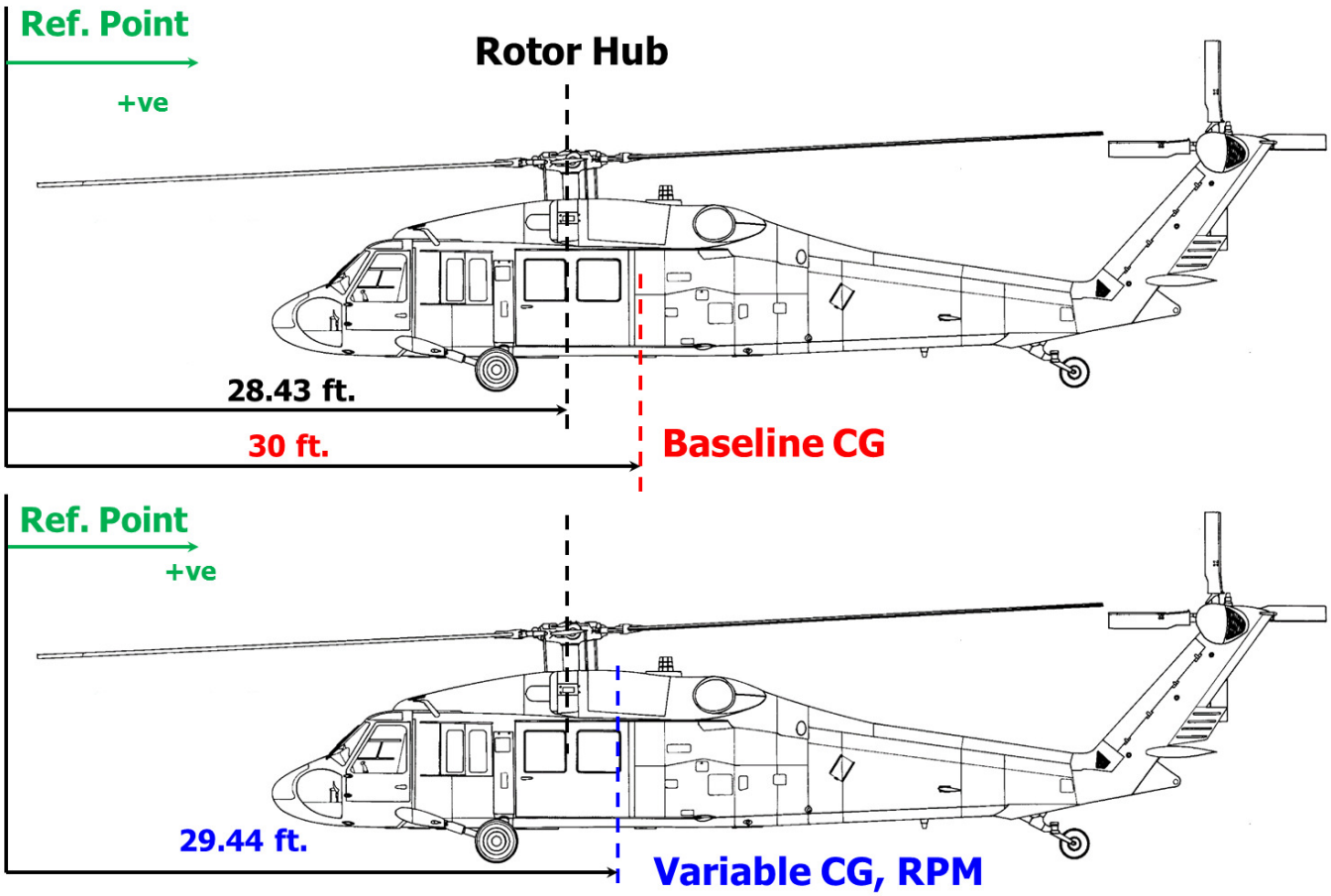

Fig. 6: Longitudinal CG position in hover

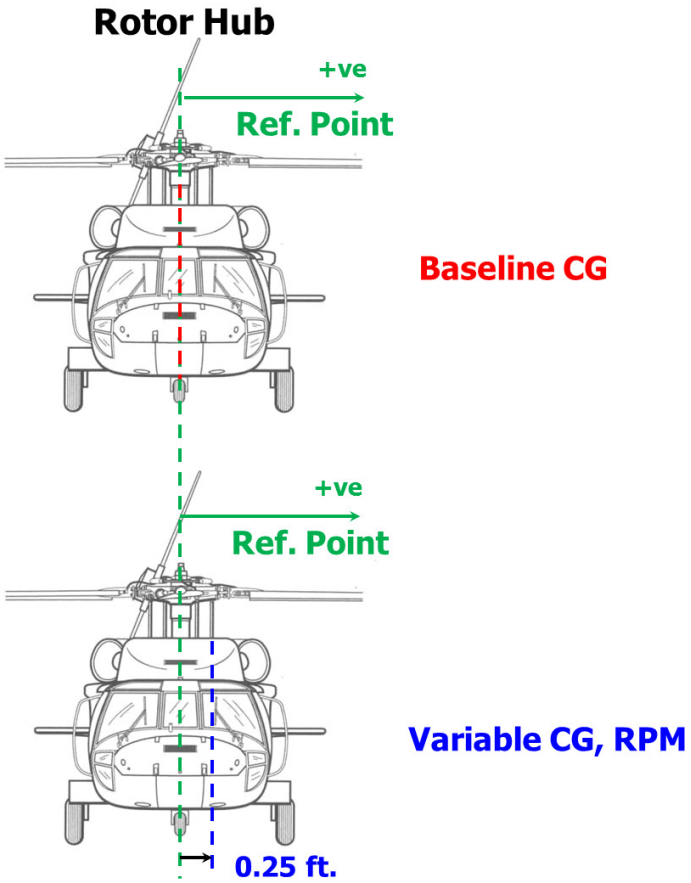

Fig. 7: Lateral CG position in hover

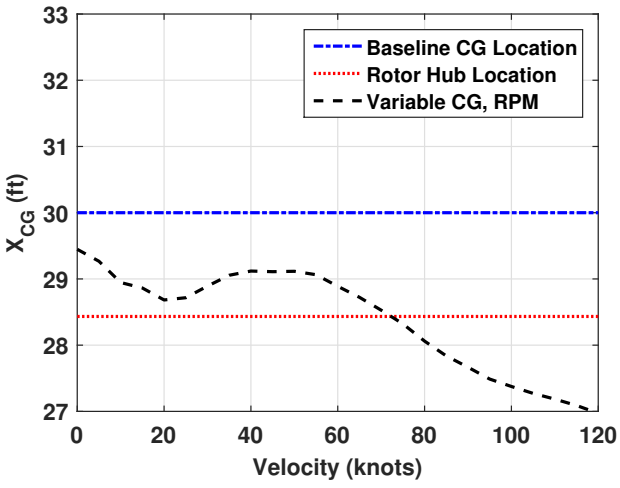

(a) Longitudinal CG Position

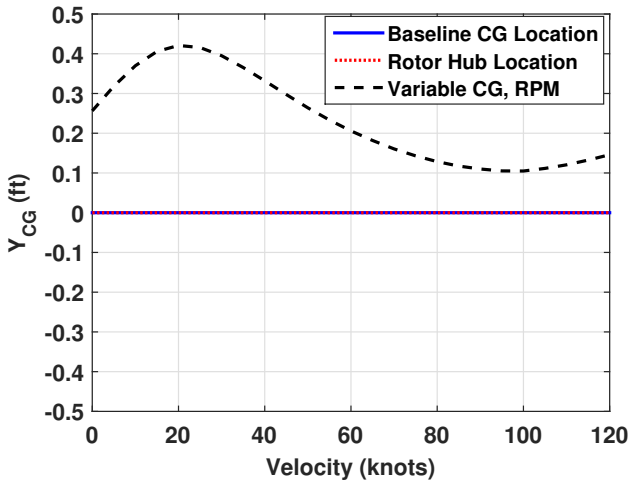

(b) Lateral CG Position

Fig. 8: Trim Sweep - CG Position

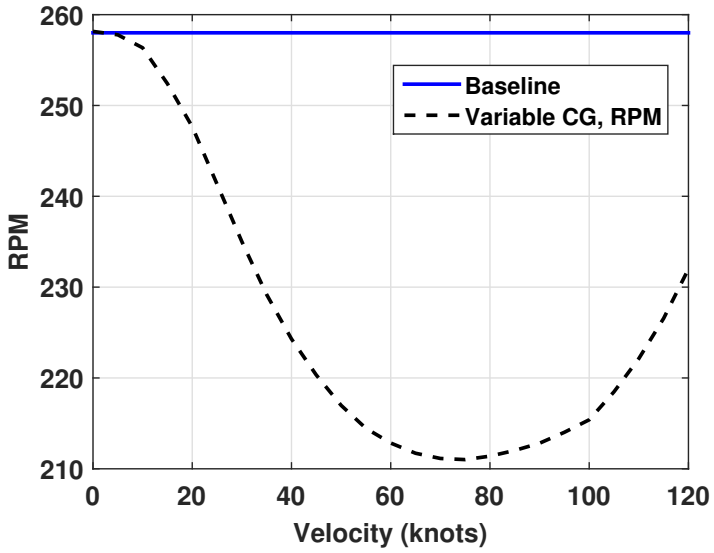

Fig. 9: Trim Sweep - RPM

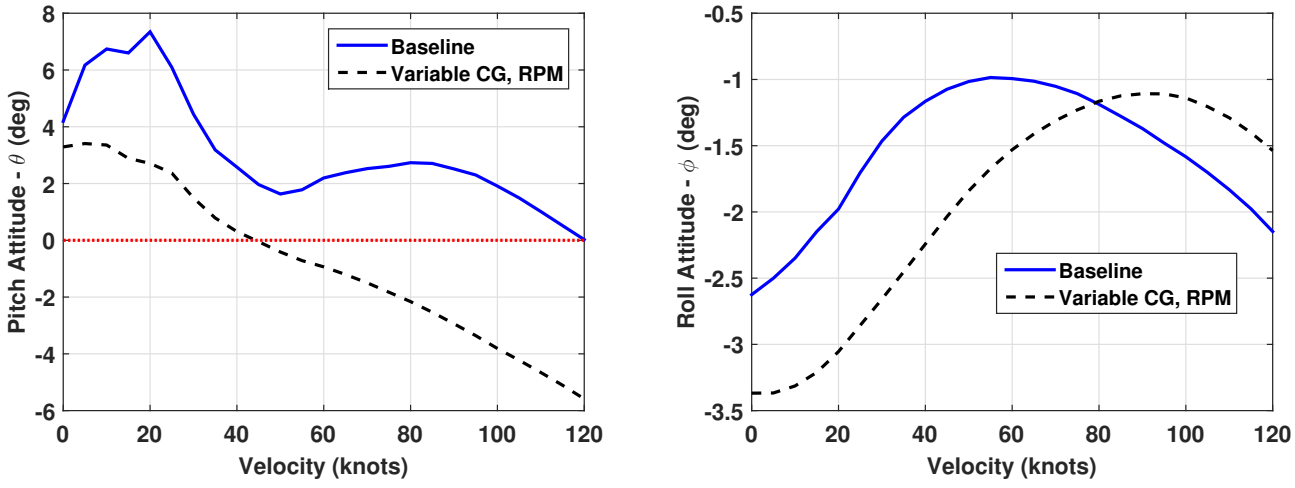

(a) Pitch Attitude

(b) Roll Attitude

Fig. 10: Trim Sweep - Attitudes

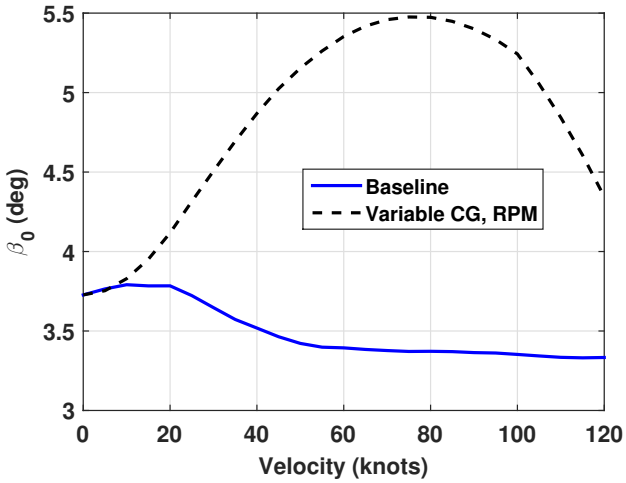

(a) Coning

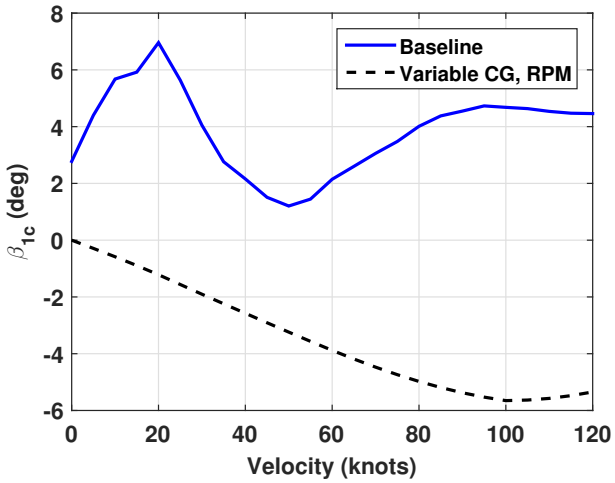

(b) Longitudinal Flapping

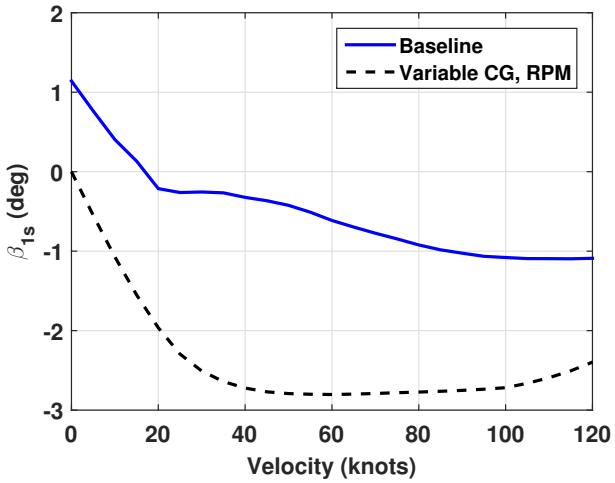

(c) Lateral Flapping

Fig. 11: Trim Sweep - Flapping

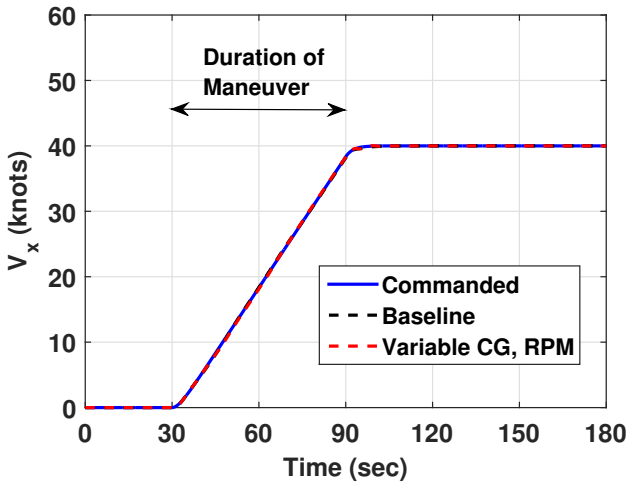

(a) Longitudinal Ground Speed

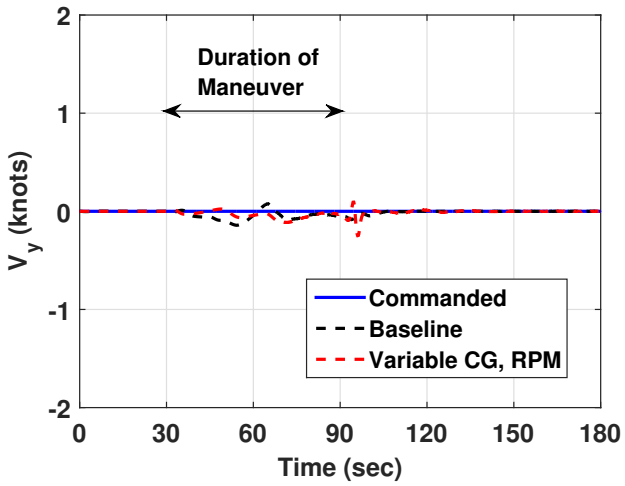

(b) Lateral Ground Speed

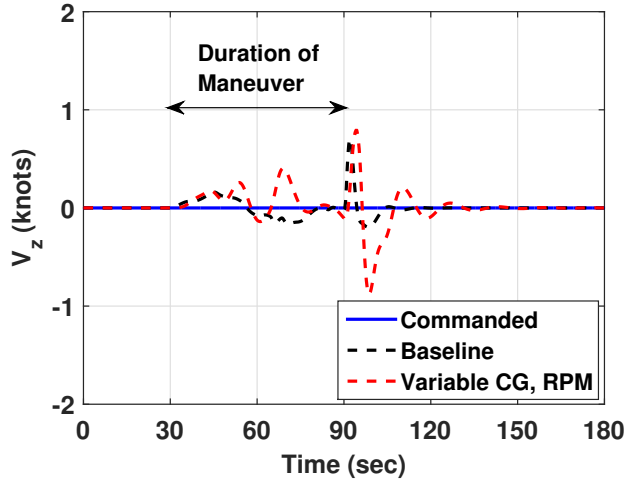

(c) Vertical Speed

Fig. 12: Hover to 40 knots - Ground Speeds

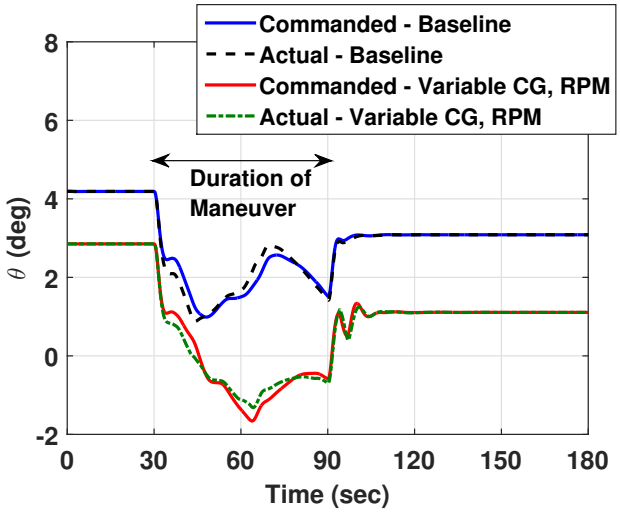

(a) Pitch Attitude

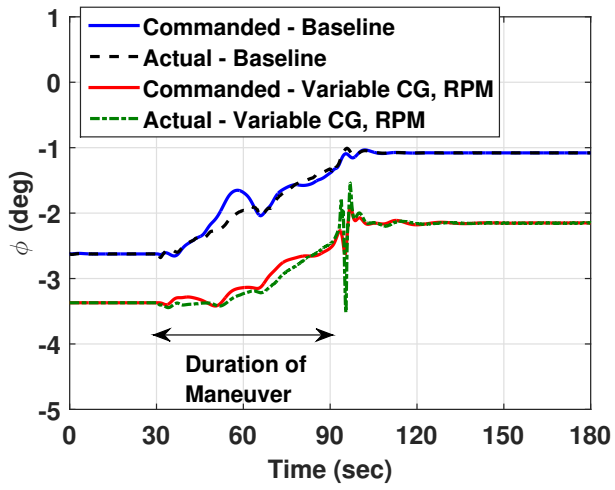

(b) Roll Attitude

Fig. 13: Hover to 40 knots - Attitudes

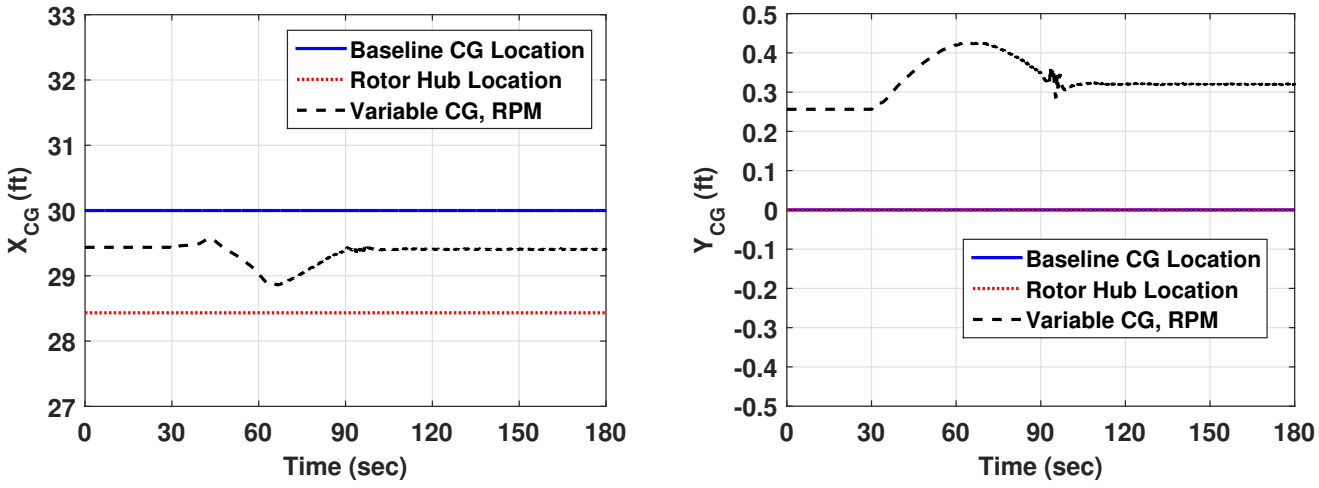

(a) Longitudinal CG Position

(b) Lateral CG Position

Fig. 14: Hover to 40 knots - CG Position

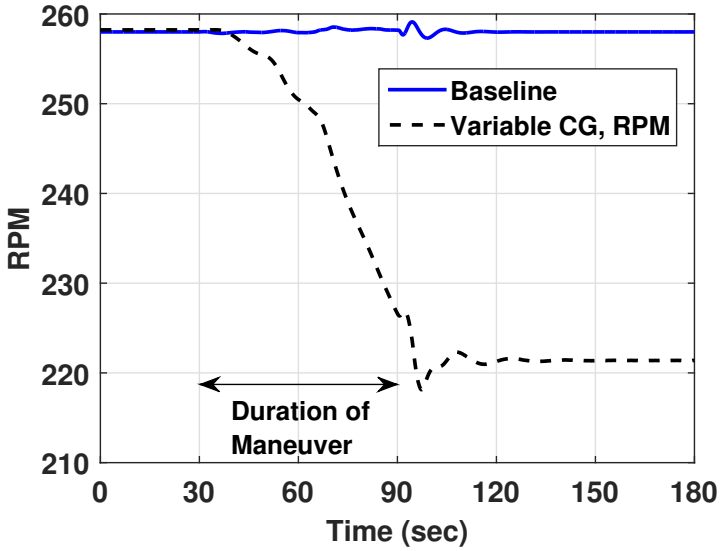

Fig. 15: Hover to 40 knots - RPM

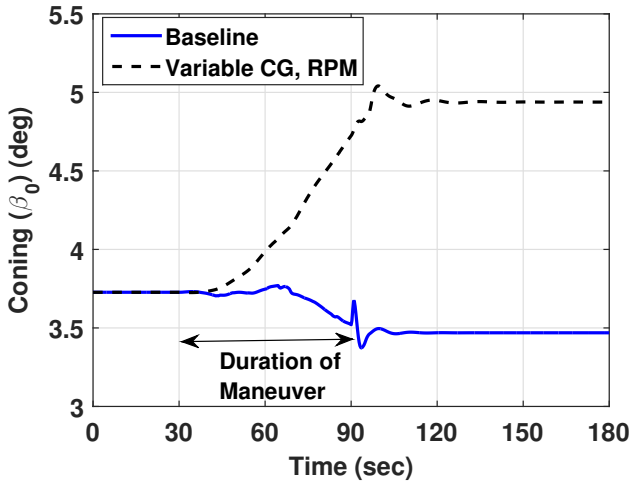

(a) Coning

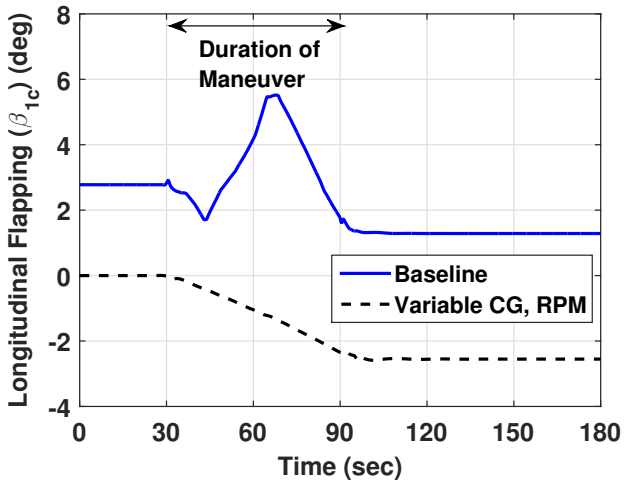

(b) Longitudinal Flapping

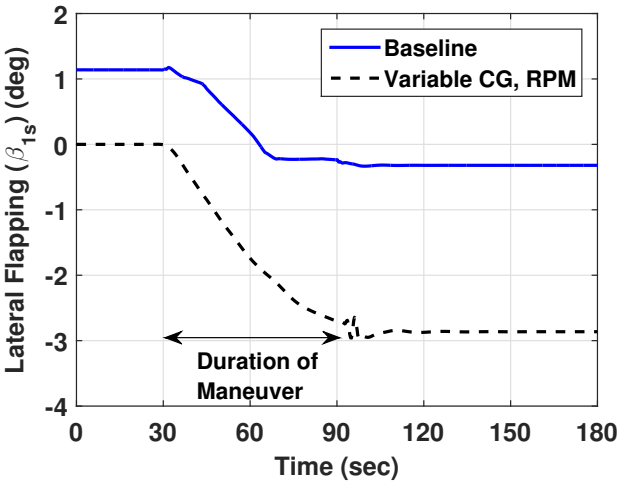

(c) Lateral Flapping

Fig. 16: Hover to 40 knots - Flapping

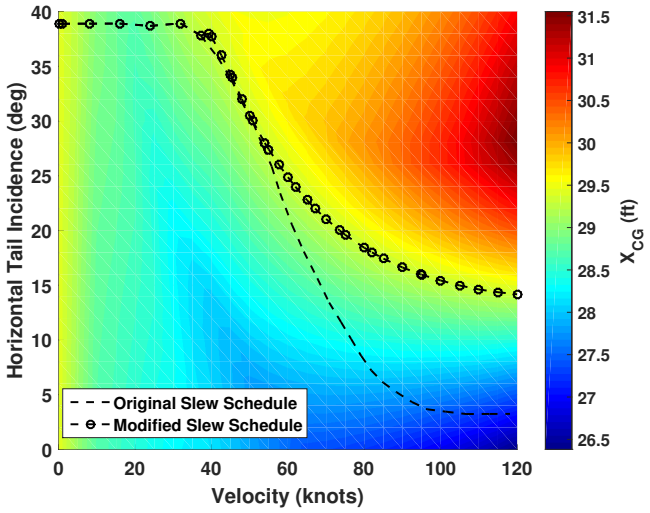

(a) Horizontal Tail Incidence and Velocity Sweep

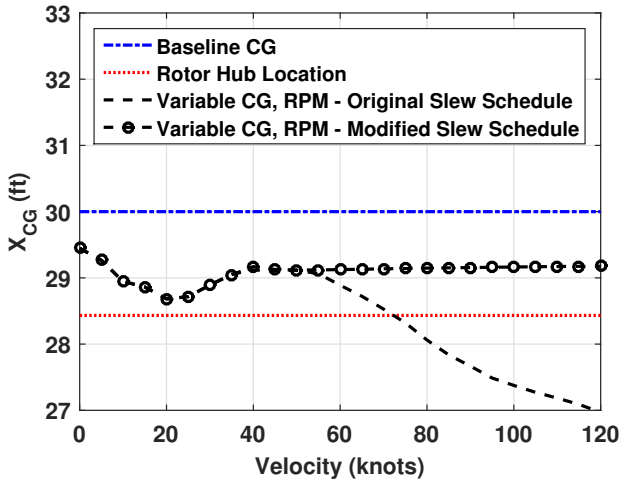

(b) Trim Sweep - Original vs Modified Slew Schedule

Fig. 17: Slew Schedule Modification - Longitudinal CG Movement

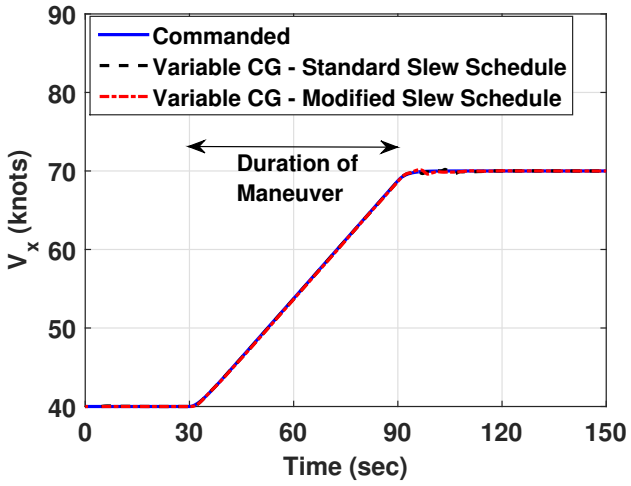

(a) Longitudinal Ground Speed

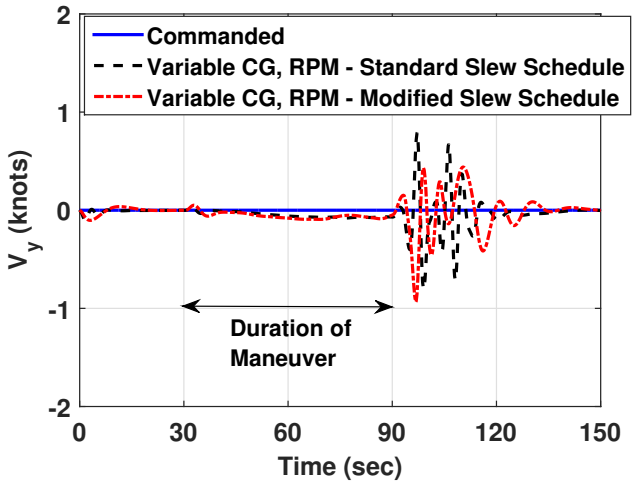

(b) Lateral Ground Speed

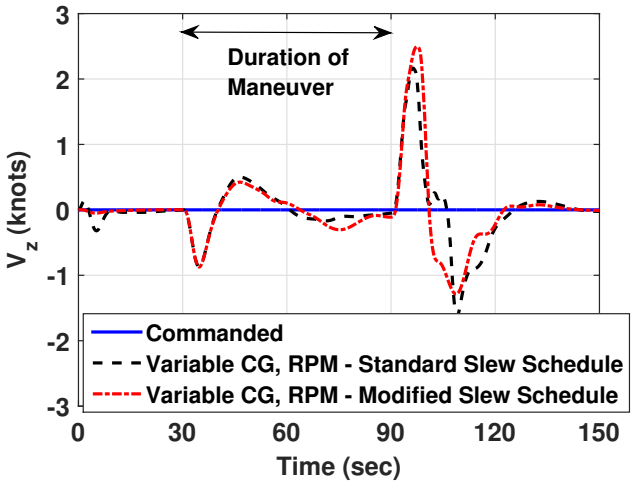

(c) Vertical Speed

Fig. 18: 40 to 70 knots - Ground Speeds

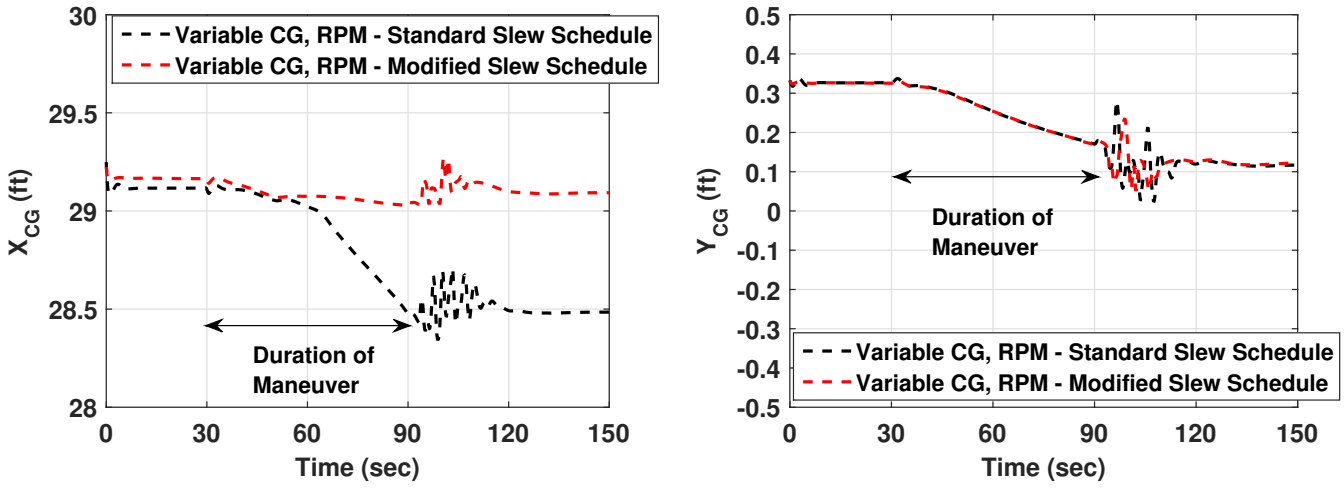

(a) Longitudinal CG Position

(b) Lateral CG Position

Fig. 19: 40 to 70 knots - CG Position

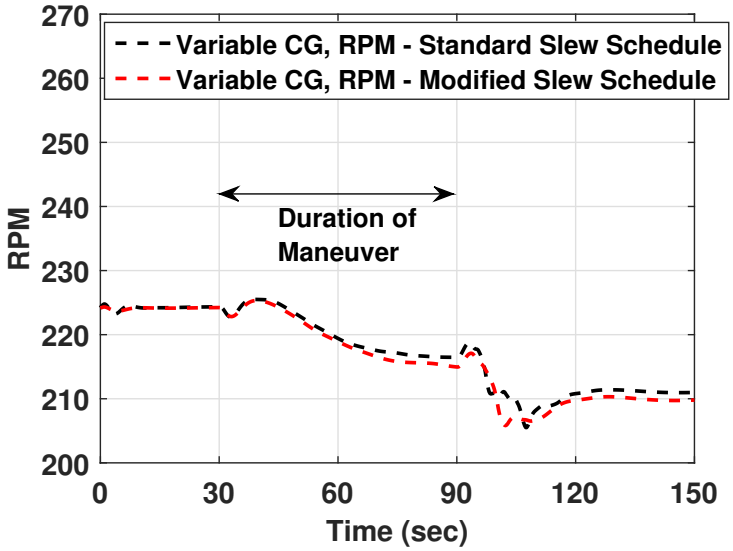

Fig. 20: 40 to 70 knots - RPM

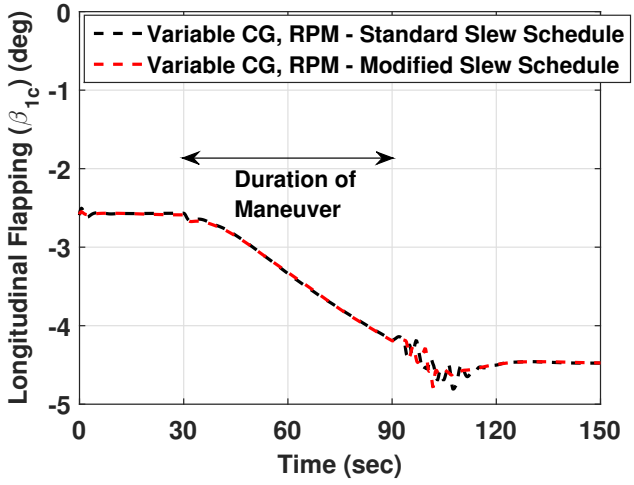

Fig. 21: 40 to 70 knots - Longitudinal Flapping